Nanoscale

PAPER

View Article Online
View Journal | View Issue

Nanostructured carbon materials based electrothermal air pump actuators†

Cite this: *Nanoscale*, 2014, **6**, 6932

Qing Liu,[ab] Luqi Liu,*[a] Jun Kuang,[ab] Zhaohe Dai,[ab] Jinhua Han[ab] and Zhong Zhang*[a]

Received 27th January 2014
Accepted 8th April 2014

DOI: 10.1039/c4nr00536h

www.rsc.org/nanoscale

Actuator materials can directly convert different types of energy into mechanical energy. In this work, we designed and fabricated electrothermal air pump-type actuators by utilization of various nanostructured carbon materials, including single wall carbon nanotubes (SWCNTs), reduced graphene oxide (r-GO), and graphene oxide (GO)/SWCNT hybrid films as heating elements to transfer electrical stimulus into thermal energy, and finally convert it into mechanical energy. Both the actuation displacement and working temperature of the actuator films show the monotonically increasing trend with increasing driving voltage within the actuation process. Compared with common polymer nanocomposites based electrothermal actuators, our actuators exhibited better actuation performances with a low driving voltage (<10 V), large generated stress (tens of MPa), high gravimetric density (tens of J kg^{-1}), and short response time (few hundreds of milliseconds). Besides that, the pump actuators exhibited excellent stability under cyclic actuation tests. Among these actuators, a relatively larger actuation strain was obtained for the r-GO film actuator due to the intrinsic gas-impermeability nature of graphene platelets. In addition, the high modulus of the r-GO and GO/SWCNT films also guaranteed the large generated stress and high work density. Specifically, the generated stress and gravimetric work density of the GO/SWCNT hybrid film actuator could reach up to more than 50 MPa and 30 J kg^{-1}, respectively, under a driving voltage of 10 V. The resulting stress value is at least two orders of magnitude higher than that of natural muscles (~0.4 MPa).

Introduction

Actuator materials that can directly convert various energies to mechanical energy have shown great potential in artificial muscles, robotics and biomedical fields.[1–5] Among them, electroactive polymers (EAPs) have attracted great attention in recent decades due to the merits of lightweight, high flexibility, and large actuation strain in response to electrical stimulation.[2] Determined by the actuation mechanisms, EAPs based actuators can be broadly divided into two categories: ionic and electric-field driven EAPs. In the ionic classification, the EAPs (*e.g.* conducting polymers, ionic polymer metal composites) are mostly actuated under relatively lower driving voltage, but the harsh working environment (electrolyte solutions or certain environmental humidity) severely restricts their broad applications.[6,7] In the meantime, electronic EAPs (including elastomers and dielectric polymers *etc.*) can work in air and exhibit large actuation strain, quick response in the order of milliseconds, and high energy densities. However, owing to low dielectric constants relative to ceramics, high electrical fields (as high as 1.3×10^8 V m^{-1}) are generally required and the force output is relatively low, which further challenges widespread utilizations.[8,9] Recently, the reduced electric-fields by up to two orders of magnitude were realized in various polymer systems through the inclusion of CNT additives.[10,11] To further reduce the magnitude of the electric field required to induce actuation, polymer nanocomposite electrothermal actuators, such as CNT/polydimethylsiloxane (PDMS) and conductive carbon nanoparticle/Nafion composites were developed.[12–14] In such cases, the electric field could be reduced to as low as $\sim 1.5 \times 10^3$ V m^{-1}. The actuation mechanism is attributed to thermal expansion of the polymers resulting from Joule heating once an external voltage is applied to the samples. In general, elastomers and soft materials with large thermal expansion coefficients will exhibit large actuation strains. However, there are still a few drawbacks for the applications of such kinds of nanocomposite electrothermal actuators, particular for the soft material based nanocomposites, as summarized below: (1) the force output greatly depends on the tensile modulus of the polymer matrix, and a low force output was observed for rubbery based nanocomposites; (2) the relatively long response time on the level of seconds; (3) the polymer matrix would be degraded due to the heat generated by the electric current, and

[a]*National Center for Nanoscience and Technology, Beijing, 100190, P. R. China. E-mail: zhong.zhang@nanoctr.cn; liulq@nanoctr.cn; Fax: +86-10-8254-5586; +86-10-6265-6765; Tel: +86-10-8254-5586; +86-10-8254-5587*

[b]*University of Chinese Academy of Science, Beijing, 100049, P. R. China*

† Electronic supplementary information (ESI) available: A movie showing the weight-lifting actuation process of the GO/SWCNT actuator. See DOI: 10.1039/c4nr00536h

then lead to deterioration of the actuation performances. Later, Vaia *et al.* proposed to utilize a CNT based thermoplastic polyimide nanocomposite as the electrothermal actuator material to improve the force output and thermal stability of actuator materials.[15] However, owing to a relatively high material stiffness (~2.5 GPa) and low conductivity (0.02 S cm^{-1}), the high driving voltage of up to 1000 V and electric field ~3.6 × 10^4 V m^{-1} were required to drive the actuators.

To realize low driving voltage while maintaining a large force output and thermal stability of electrothermal actuator materials, in this work, we designed and fabricated an air pump-type electrothermal actuator by utilizing nanostructured carbon materials including SWCNT and graphene as building and heating elements. The actuation mechanism of the air pump-type electrothermal actuator is based on the volume expansion of the entrapped air once an electric current flows through the materials. According to the mechanism, gas-impermeability of the actuator material against air diffusion is required to maximize the actuation performance. It has been reported that graphene and GO platelets could act as perfect two dimensional gas-barriers against diffusion of liquids, vapours and gases, and thus air permeation and leakage during the actuation process could be hindered effectively.[16–18] Besides that, earlier works have demonstrated that free-stranding nanostructured carbon material films (such as the SWCNT, graphene and GO/CNT hybrid films) possess good electric conductivities, high tensile modulus, and thermal stability.[19–22] Consequently, low driving voltage and large force outputs are expected for the air pump electrothermal actuators by employing various nanostructured carbon material films as actuator materials. Experimental results demonstrated that the generated stress for GO/SWCNT hybrid film actuators could reach up to 50 MPa at a 10 V driving voltage, which is at least two orders of magnitude higher than that of CNT/PDMS nanocomposite electrothermal actuators.[14] Moreover, in contrast to thermal bimorph actuators which are composed of two materials with different thermal expansion coefficients,[23] our air pump-type actuator is simple to design and fabricate in lab and no micro-processing is demanded. Our work will be helpful not only to guide the design and fabrication of new-style actuators based on various nanostructured carbon materials, but also to deeply understand the microstructures influence of materials on actuation performances for air pump-type electromechanical actuators.

Experimental section

SWCNTs (purity >95%, average diameter <1.6 nm) were purchased from Chengdu Organic Chemical Co. Ltd. For the SWCNT dispersion, 30 mg SWCNT was mixed with 600 mg Triton X-100 and 100 ml DI water, then subjected to ultrasonication for 20 minutes under 400 W power in an ice bath (2 s on and 2 s off), the mixture was then centrifuged to remove the aggregates (4500 rpm for 30 min). The supernatant dispersion was collected and utilized as the starting material to prepare pure SWCNT films. GO was prepared from purified natural graphite by the modified Hummers method according to a previous study.[24] The obtained GO solution was diluted to 0.2 mg ml^{-1} for the film preparation. For the GO/SWCNT hybrid solution preparation, 5 mg SWCNT and 100 mg Triton X-100 were first added into 100 ml GO solution (0.2 mg ml^{-1}), and then the mixture was subjected to ultrasonication and centrifugation to get the final homogeneous supernatant. The SWCNT, GO and GO/SWCNT films were prepared by filtrating 20 ml solution through a cellulose membrane filter (47 mm in diameter, 0.22 μm pore size). For the SWCNT and GO/SWCNT films filtration, 300 ml DI water was used to remove the surfactant. After air drying, the resulting films were peeled off from the membranes. The SWCNT and GO/SWCNT films were used as prepared without any further treatment while GO films were reduced as referred to Cheng's work by utilizing hydroiodic acid (HI) as a reducing agent.[25] To avoid the damage of r-GO films during the reduction process, HI vapour was used instead of HI solution. After reduction, the r-GO films were washed with DI water and ethanol to remove the residual HI and I_2. The density of different carbon material films were measured by using the weighing method and the final results were 0.9, 2.0, and 1.5 × 10^3 kg m^{-3} for the SWCNT, r-GO, and GO/SWCNT, respectively.

The morphology of the as-prepared SWCNT, GO, r-GO and GO/SWCNT films was studied using a Scanning Electron Microscope (SEM, HITACHI S-4800). A dynamic mechanical analyzer (TA, DMA Q800) was employed to evaluate the mechanical properties of the resulting films. The films were cut into strips with a width of 2 mm, and the gauge length was controlled to be 10.0 ± 0.5 mm. The static tensile tests were conducted in the displacement ramp mode with a pre-strain 0.01% and a ramp rate 20 μm min^{-1}. At least 5 samples were tested. The electrical property was tested using a Keithley 4200 instrument by the 4-probe method.

The pump-type actuators were prepared as following: polytetrafluoroethylene (PTFE) boxes (length × width × depth is 15 × 15 × 10 mm) with one end open were first machined, and then carbon material films were glued onto the top of the boxes to seal the air inside. Two pieces of copper conductive strips were pasted on the films as electrodes. The electrical power was supplied using a Tektronix Arbitrary Function Generator (AFG3011), and the displacement was measured using a LK-G5001 laser displacement sensor. The laser was concentrated on the centre of the carbon material films to detect the displacement change. The temperature of the materials when the actuation deformation reached the maximum during the actuation process was measured using a laser sight infrared thermometer with a resolution of 0.1 °C.

Results and discussion

Fig. 1a shows the schematic drawing of the air pump-type electrothermal actuator we designed, in which various nanostructured carbon material films were utilized as heating elements. When a driving voltage is applied, an electric current immediately flows through the film, and the heat generated due to Joule heating leads to expansion of the sealed air. Subsequently, the film would be plumped up, and reach the maximum deformation. Once the voltage is cut off, the heat

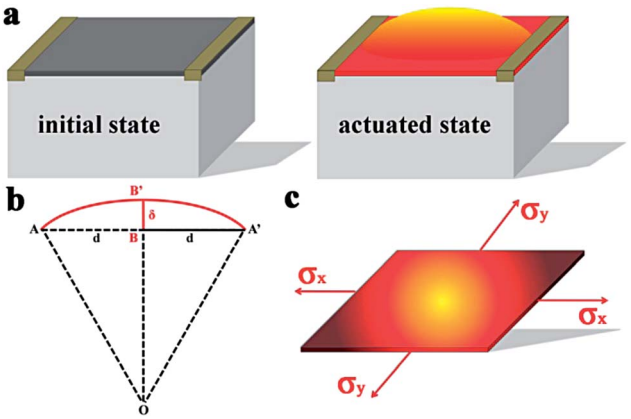

Fig. 1 (a) Depiction of the initial and actuated state of an air pump-type electrothermal actuator; (b) strain calculation depiction; (c) stress condition of the carbon material film under the actuated state.

generation is stopped immediately, and the film would recover to the initial state accompanied by the air contraction. In general, the heat generated by the carbon material film at a given time period greatly depends on the driving voltage, electrical conductivity, and sample size.[15] The thermal energy generated would enhance greatly with increasing driving voltages and electrical conductivity of materials, and eventually lead to effective air expansion. Moreover, considering the air expansion dominated actuation mechanism of our air pump-type actuator, the carbon material films with a better gas-barrier property would efficiently hinder air permeation and leakage during the actuation process, and result in an improved actuation stroke. Earlier works have proven that individual graphene sheets and its nanocomposites behaved good in terms of gas-impermeability due to its planar feature.[16–18,26] Meanwhile, the air volume sealed inside box also would affect the actuator performance at a given driving voltage. The air with a small volume could be expanded more effectively, and eventually lead to a large actuator stroke. However, it is not under consideration in this work. Herein, the boxes were machined with the same dimensions to make the air volume influence on the actuation performance negligible.

In this work, GO and SWCNT were used as building blocks to fabricate various nanostructured carbon material films. All films were prepared *via* an environmental friendly method called vacuum-assisted self-assembly filtration we used before.[24] To illustrate the influence of various carbon material film microstructures on the actuation performance, herein, three kinds of carbon material films were prepared in the lab including SWCNT, r-GO and GO/SWCNT hybrid films. For comparison, the thickness of all the films was controlled in the range of 1.5–3.0 μm. Fig. 2 shows digital images of the as-prepared SWCNT, GO, r-GO, and GO/SWCNT hybrid films with the diameter of about 40 mm. A four-probe electrical test indicated that the conductivities of SWCNT, r-GO, and GO/SWCNT films were 120, 80 and 75 S cm^{-1}, respectively.

Fig. 3a and b show the SEM cross-sectional and top view of the as-prepared SWCNT film. The film has a laminar structure with entangled nanotubes to form a network structure through

Fig. 2 Digital images of the as-prepared SWCNT, GO, r-GO and GO/SWCNT hybrid films.

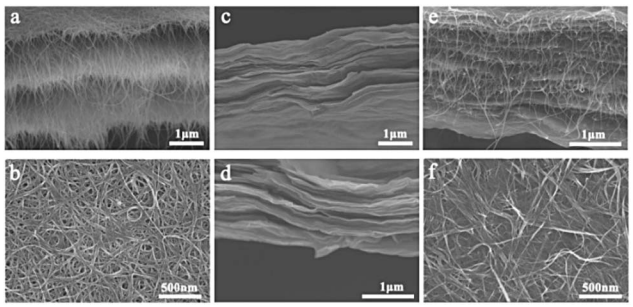

Fig. 3 SEM images of (a and b) cross-sectional and top view of the SWCNT film; (c and d) cross-sectional view of the GO and the r-GO film; (e and f) cross-sectional and top view of the GO/SWCNT hybrid film.

van der Waals forces at tube–tube junctions, which would endow the film high electrical conductivity as well as mesoporous microstructures. The presence of the mesoporous microstructure of the SWCNT enables the electrolyte infiltrate efficiently during the charge and discharge process, which eventually leads to enhanced actuation performance for the ionic-type actuator.[27] However, on the other hand, the presence of mesopores in the SWCNT film would greatly deteriorate actuation performance of the air pump-type actuator due to air diffusion. Comparatively, Fig. 3c shows that GO platelets were alternatively piled up to form a uniform layered structure, which was consistent with our previous work.[24] Such a well-packed layered microstructure was still maintained after further chemical reduction (Fig. 3d). Fig. 3e presents the cross-sectional view of the layered GO/SWCNT hybrid film. Earlier work has pointed out that the presence of nanotubes will not greatly influence the self-assembly process of GO individual platelets during the vacuum-assisted filtration process. The main reason is due to the attachment of the CNT onto GO platelets through π–π stacking interaction between the delocalized electrons in the aromatic regions of GO sheets and the CNT in the mixed suspensions.[28] Different from the mesoporous structures of the SWCNT film, no apparent mesopores were observed in the hybrid films as shown in Fig. 3f. Consequently, due to the highly dense packing feature of the r-GO and the GO/SWCNT hybrid film together with the perfect gas-impermeable nature of individual graphene and GO nanosheets, these films are expected to exhibit excellent actuation performance.

For conventional EAP materials, the force generation is greatly limited by the modulus of actuator materials. Many

studies have shown that the maximum stress that can be sustained by conventional EAPs during actuation appeared to be less than 10 MPa.[8,29,30] Additionally, the low stress generation from conductive polymers implies that the application of mechanical amplifiers is also very limited. Alternatively, graphene and its hybrid films have shown superior mechanical properties, which show great potential in these fields. Fig. 4 shows the typical tensile stress–strain curves of carbon material films. Briefly speaking, the average tensile modulus and strength of various carbon material films are much higher than that of conducting polymers. Tensile tests indicated that the modulus was 3.2 ± 0.45 GPa and 6.0 ± 0.53 GPa for the SWCNT and r-GO films, respectively. After combining GO platelets with SWCNT, the modulus of the hybrid film was increased from initial 10.6 ± 0.95 GPa for the GO film to 15.2 ± 0.34 GPa, demonstrating an improvement of about 40%. Theoretical simulations based on first-principles calculation have demonstrated that there are two major factors to determine the overall mechanical properties of the GO film, namely the inter-layer and intra-layer interaction.[31] Herein, we speculate that the mechanical enhancement of the hybrid film may result from the increased intra-layer interaction, in which the SWCNT with a large aspect ratio on the order of 10^3 could easily intra-link the adjacent GO sheets during the vacuum-assisted filtration process. Consequently, the increased intra-layer integration of GO platelets would benefit effectively the load transfer along the in-plane direction, and then the tensile modulus was improved. In addition, considering the fact that both output stress and work density of actuators greatly depend on the modulus of actuator materials, therefore, the improvement of actuation performances is expected for the GO/SWCNT hybrid films. We will discuss it later.

The actuation performances of various carbon material films were tested under various square wave potentials with the frequency of 0.1 Hz. Fig. 5a shows the actuation displacement of the three actuators under a 10 V driving voltage. As seen, the films were promptly plumped up as the voltage was applied, and the deformation would be kept steady during the electric stimulation process, which indicates the equilibrium between heat generation and dissipation. Once the voltage was cut off,

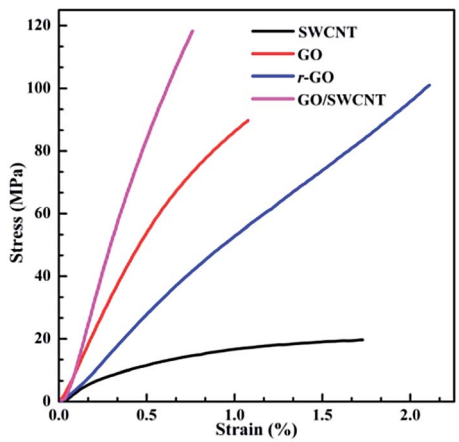

Fig. 4 Typical stress–strain curves of the as-prepared SWCNT, GO, r-GO and GO/SWCNT films.

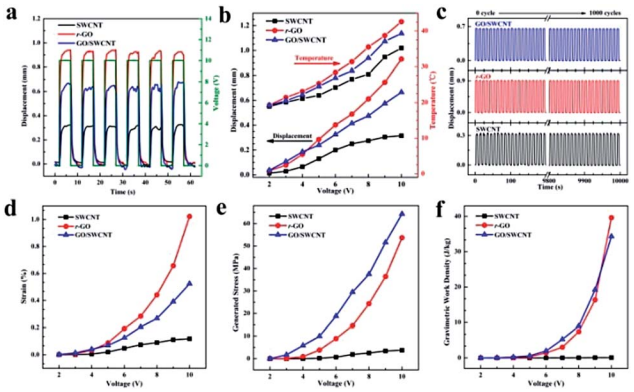

Fig. 5 (a) Actuation displacement of pump actuators under a 10 V driving voltage; (b) working temperature and displacement as a function of driving voltages; (c) cyclic actuation displacement under a 10 V driving voltage; (d) actuation strain, (e) generated stress and (f) gravimetric work density of pump actuators as a function of driving voltages.

the film would simultaneously recover to its original state. Among the three actuator materials, the r-GO film showed the highest deformation up to 0.93 mm, whereas the values for GO/SWCNT and SWCNT films were 0.68 mm and 0.32 mm, respectively. Fig. 5b summarizes the actuation displacement and working temperature of the nanostructured carbon material films during the actuation process as a function of the driving voltage. Upon increasing the driving voltage, larger electric currents flowed through carbon material films, and then more thermal energy could be generated to induce air expansion efficiently. Consequently, the actuation displacement and working temperature would exhibit a monotonically increasing trend with the driving voltage prior to the structural failure of actuator films. For instance, the working temperature for the r-GO, GO/SWCNT and SCWNT films under a 10 V driving voltage was 42.6, 39.3, and 35.2 °C, respectively. Among the three actuator films, the r-GO film exhibited the largest displacement as well as the highest temperature at a given driving voltage. The repeatability and stability of the actuators were investigated by cyclic actuation under a 10 V driving voltage as shown in Fig. 5c. It is found that, the displacement could be maintained during the cyclic actuation process for more than 1000 cycles, indicating the long time working life of nanostructured carbon materials based pump actuators.

To quantitatively define the actuator strain, the plumped film is simplified as a dome once the deformation of the film reached the maximum, as presented in Fig. 1b. The actuation strain ε can be calculated by eqn (1), in which d stands for the half length of the film, and δ represents the actuation displacement of the film from the initial state.

$$\varepsilon = \frac{(d^2+\delta^2)\left[\tan^{-1}\left(\frac{2d\delta}{d^2-\delta^2}\right)\right]}{2d\delta} - 1 \quad (1)$$

Fig. 5d summarizes the derived actuation strain of the actuators as a function of the applied voltage. It can be clearly

seen that the strain shows an apparently increasing trend with the driving voltage. Among the three carbon material films, the r-GO film exhibits the largest strain, whereas the SWCNT film possesses the smallest one within the whole driving voltage range. Specifically, the actuation strain of the r-GO film was about 1.02% at a 10 V driving voltage, which is approximately one order of magnitude higher than that of the SWCNT film (0.12%), and the actuation strain of the GO/SWCNT film is located in the middle (0.52%).

As known, the magnitude of the actuation stroke is mainly determined by the thermal energy generated and mechanical properties of actuator materials. Material with higher electrical conductivity would generate more heat according to the Joule effect, and materials with a lower modulus would be deformed much more easily. Thus, the SWCNT film with the highest electrical conductivity (120 S cm^{-1}) and the lowest tensile modulus (3 GPa) is speculated to exhibit the largest actuation displacement and strain among the three carbon material films. However, experimentally, the SWCNT film actuator exhibited the smallest actuation displacement and strain under various driving voltages. This phenomenon should be attributed to the presence of the mesoporous microstructure of the SWCNT films as presented in Fig. 3b, in which the air leakage easily occurred during the electrical stimulus process. Thus, the efficient heat dissipation led to the relative low working temperature for the SWCNT film as presented in Fig. 5b. Conversely, the excellent gas-impermeability of r-GO platelets efficiently hindered the air diffusion during the actuation process and thereby the r-GO film exhibited the largest actuation deformation. In addition, compared to the maximum displacement of the CNT/PDMS nanocomposite (~1.1 cm at 10 V), the displacement amplitudes of the r-GO actuator showed the same level under a 10 V stimulus.[12,14] But, a larger output force is expected for the r-GO actuators due to the higher modulus on the level of GPa *versus* that of MPa for CNT/PDMS nanocomposites. Given that the actuation strain of tested actuator materials within the elastic deformation range, the generated stress of the actuator at a given driving voltage could be further derived from the typical tensile stress–strain curves of the carbon material films (Fig. 4). Fig. 5e presents the generated stress as a function of the applied voltage. Specifically, at a 10 V driving voltage, the generated stresses for the SWCNT, r-GO and GO/SWCNT films were 3.75 MPa, 53.7 MPa and 64.3 MPa respectively. Comparatively, the generated stress of the hybrid film is at least two orders of magnitude higher than that of CNT/PDMS nanocomposites at 52 V.[14] Even though the actuation strain of the GO/SWCNT hybrid film was smaller than that of the r-GO film, the relatively higher modulus rendered the hybrid film to generate a larger stress. To further examine the weight-lifting performance of the actuator, a piece of the PDMS film (280 mg) which is about 300 times heavier than the weight of the GO/SWCNT film was placed on the top of the actuator, as shown in Fig. 6a. It is found that the PDMS film could be lifted upward when a driving voltage was applied (a movie showing the actuation process is available in the ESI†). Fig. 6b shows the actuation displacement at 8 V driving voltage with a frequency of 0.01 Hz. It was found that the actuation displacement (0.425 mm) could be approximately the same as the load-free actuation displacement (0.475 mm), which confirms the excellent stress output property of the GO/SWCNT actuator. It should also be noticed that, compared with the actuation process without the load, it would take much more time to reach the maximum displacement due to the weight lifting. Once the driving voltage was cut off, the heat generation would be stopped simultaneously. Subsequently, the actuator film slowly recovered to its initial state. Such retardance of the displacement was attributed to the impeded heat dissipation induced by PDMS, thus much more time was required to get recovery. The cyclic experiment was carried out to examine the working life of the actuators under the loading condition. It is found that, after long time cyclic actuation, the actuation performance was still maintained (as shown in Fig. 6c), which implied the excellent loading capability of the actuator.

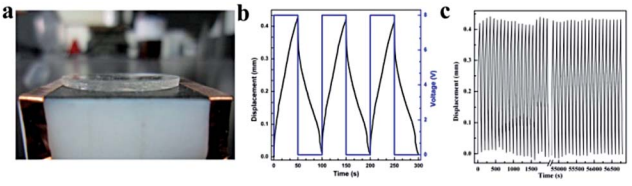

Fig. 6 (a) Optical image of the weight-lifting test of the GO/SWCNT hybrid film actuator; (b) actuation displacement under a 8 V driving voltage with 300 times higher load; (c) cyclic weight-lifting actuation performance.

With the assumption that the plumped film underwent a uniform plane stress state as described in Fig. 1c, the gravimetric work density (p) could be obtained by eqn (2), in which E and ν mean Young's modulus and Poisson's ratio of the materials respectively, and ρ is the mass density of the materials.

$$P = \left(\frac{E}{1-\nu}\varepsilon^2\right) \quad (2)$$

The gravimetric work density of actuators derived from eqn (2) shows a monotonic enhancement with increasing driving voltage, as presented in Fig. 5f. Comparatively, the enhanced trend of r-GO and GO/SWCNT actuators is much more significant than that of the SWCNT actuator. Specifically, the gravimetric work density for r-GO and GO/SWCNT actuators was 39.6 and 34.3 J kg^{-1} respectively at 10 V, which is more than 500 times higher than that of the SWCNT actuator (0.06 J kg^{-1}). Such significant improvement could be attributed to both the larger actuation strain and higher modulus of the r-GO and the GO/SWCNT films. Earlier work done by Baughman *et al.* has shown a large work capacity (30 J kg^{-1}) obtained for CNT aerogel sheets actuated under a 1.6 kV driving voltage.[32] Herein, a much lower driving voltage (10 V) was required to achieve the comparable work density by using r-GO or the GO/SWCNT film based pump-type electrothermal actuators.

Apart from the actuation strain, generated stress and gravimetric work density as discussed above, the response time is another important parameter to evaluate the actuator performances. Herein, the response and recovery time of the actuators

were derived using the curve fitting based on the following equations:

$$\delta(t) = \delta_0\left(1 - e^{-\frac{t}{t_0}}\right) \quad (3)$$

$$\delta(t) = \delta_1 + \delta_0 e^{-\frac{t}{t_1}} \quad (4)$$

In the equations, δ represents the actuation displacement at time t, δ_0 relates to the maximum actuation displacement, and δ_1 is the residual actuation displacement during the recovery process, t_0 and t_1 stand for the response and recovery time respectively. Fig. 7a and b present the curve fitting results of different actuator materials at a 10 V driving voltage. It can be clearly seen that eqn (3) and (4) fitted well with the response and recovery curves. The response and recovery time of r-GO, SWCNT and GO/SWCNT actuators are summarized in Table 1. Apparently, the response and recovery time of all actuator materials are within the range of few hundreds of ms, which is at least one order of magnitude shorter than that of the CNT/polymer nanocomposite electrothermal actuators (response time ranged from few seconds to several tens of seconds).[12] According to a previous study, the quality factor, $C_p\rho/\sigma$, was proposed to define the speed with which a material can be heated *via* an electric current, where C_p, ρ and σ are the specific heat capacity, density and electrical conductivity of the material, respectively.[15] A low quality factor implies that the material will heat more rapidly under an applied voltage.[15] In our case, the electrical conductivity of the actuator materials is in the range of 70–120 S cm^{-1}, which is at least two orders of magnitude higher than that of polymer nanocomposites. The quick response of our pump actuator could be attributed to the high electrical conductivity of carbon material films. Once the voltage was turned on, the films would be heated spontaneously and the air would be expanded promptly. On the other hand, once the voltage was turned off, the thermal energy generation *via* the Joule heating stop immediately, and then the air would contract to the initial state. Specifically, the r-GO film actuator exhibited the fastest response and recovery speed among the three actuators, while the GO/SWCNT turned out to be slightly slower, and the SWCNT actuator exhibited the longest response and recovery time. The observed difference in the response and recovery time could be attributed to the variation in microstructures of actuator materials. The excellent response and recovery behaviors of the r-GO and GO/SWCNT film actuators are originated from the gas-impermeability of graphene and GO nanosheets. On the other hand, the SWCNT film actuator with mesoporous structures would take much more time to achieve the maximum deformation because of air permeation. Meanwhile, for a given actuator, the recovery time is quite close to the response time, further indicating a good operation stability and reproducibility of the pump-type actuators.

Table 1 Response and recovery fitting results under a 10 V driving voltage

Actuator materials	Response time	Recovery time
SWCNT	764 ms	795 ms
r-GO	308 ms	370 ms
GO/SWCNT	364 ms	414 ms
CNT/polymer (30 V DC voltage)[12]	About 20 s	About 50 s

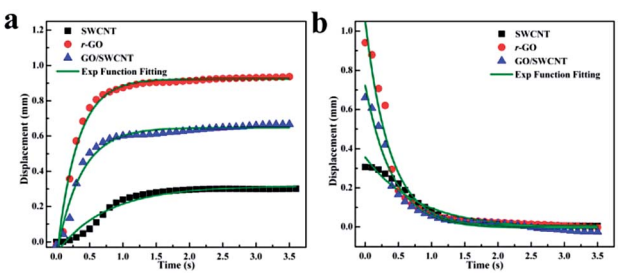

Fig. 7 (a) Response time and (b) recovery time fitting for carbon material film actuators.

Conclusion

In summary, we designed and fabricated electrothermal air pump-type actuators by utilization of SWCNT, r-GO, and GO/SWCNT as heating elements and mechanical force generators. Compared with common polymer nanocomposite electrothermal actuators, air pump-type actuators exhibited better actuation performance as well as longer service life. Specifically, under a 10 V driving voltage, the generated stress and work density could reach more than 50 MPa and 30 J kg^{-1} for the GO/SWCNT hybrid film actuator. The actuator exhibited excellent weight-lifting behaviour and stroke consistent with an external load which was about 300 times heavier than the weight of the actuator film, and demonstrated excellent loading capability for the long time cyclic actuation process. The response and recovery time of carbon material actuators are on the level of few hundreds of ms, at least one order of magnitude faster than that of electrothermal polymer nanocomposite actuators. The large generated stress together with the rapid response at a low driving voltage enable this type of actuator to be potentially applied in various aspects, such as sensor, switches, biomimetic breath equipment, and so on.

Acknowledgements

This project was jointly supported by the National Key Basic Research Program of China (Grant no. 2012CB937503 and 2013CB934203) and the National Natural Science Foundation of China (Grant no. 51173030 and 11225210).

Notes and references

1 S. Maeda, Y. Hara, T. Sakai, R. Yoshida and S. Hashimoto, *Adv. Mater.*, 2007, **19**, 3480.
2 T. Mirfakhrai, J. Madden and R. Baughman, *Mater. Today*, 2007, **10**, 30.

3 K. Cho, J. Rosmarin and H. Asada, *IEEE International Conference on Robotics and Automation*, 2007, p. 921.
4 E. Smela, *Adv. Mater.*, 2003, **15**, 481.
5 H. Jiang, S. Kelch and A. Lendlein, *Adv. Mater.*, 2006, **18**, 1471.
6 M. Shahinpoor and K. J. Kim, *Smart Mater. Struct.*, 2001, **10**, 819.
7 S. D. Deshpande, J. Kim and S. R. Yun, *Smart Mater. Struct.*, 2005, **14**, 876.
8 R. Pelrine, R. Kornbluh, Q. Pei and J. Joseph, *Science*, 2000, **287**, 836.
9 R. Shankar, T. K. Ghosh and R. J. Spontak, *Adv. Mater.*, 2007, **19**, 2218.
10 S. Zhang, N. Zhang, C. Huang, K. Ren and Q. Zhang, *Adv. Mater.*, 2005, **17**, 1897.
11 C. Park, J. H. Kang, J. S. Harrison, R. C. Costen and S. E. Lowther, *Adv. Mater.*, 2008, **20**, 2074.
12 Y. Hu, G. Wang, X. Tao and W. Chen, *Macromol. Chem. Phys.*, 2011, **212**, 1671.
13 M. Kato and M. Ishibashi, *J. Phys.: Conf. Ser.*, 2008, **127**, 012003.
14 L. Z. Chen, C. H. Liu, C. H. Hu and S. S. Fan, *Appl. Phys. Lett.*, 2008, **92**, 263104.
15 A. T. Sellinger, D. H. Wang, L. S. Tan and R. A. Vaia, *Adv. Mater.*, 2010, **22**, 3430.
16 O. Leenaerts, B. Partoens and F. M. Peeters, *Appl. Phys. Lett.*, 2008, **93**, 193107.
17 J. S. Bunch, S. S. Verbridge, J. S. Alden, A. M. van der Zande, J. M. Parpia, H. G. Craighead and P. L. McEuen, *Nano Lett.*, 2008, **8**, 2458.
18 R. R. Nair, H. A. Wu, P. N. Jayaram, I. V. Grigorieva and A. K. Geim, *Science*, 2012, **335**, 442.
19 R. H. Baughman, A. A. Zakhidov and W. A. de Heer, *Science*, 2002, **297**, 787.
20 Y. Zhu, S. Murali, W. Cai, X. Li, J. W. Suk, J. R. Potts and R. S. Ruoff, *Adv. Mater.*, 2010, **22**, 3906.
21 H. Chen, M. B. Müller, K. J. Gilmore, G. G. Wallace and D. Li, *Adv. Mater.*, 2008, **20**, 3557.
22 L. Wang, C. Li, D. Wang, Z. Dong, F. X. Zhang and J. Jin, *J. Nanosci. Nanotechnol.*, 2013, **13**, 5461.
23 S. E. Zhu, R. Shabani, J. Rho, Y. Kim, B. H. Hong, J. H. Ahn and H. J. Cho, *Nano Lett.*, 2011, **11**, 977.
24 Y. Gao, L. Q. Liu, S.-Z. Zu, K. Peng, D. Zhou, B. H. Han and Z. Zhang, *ACS Nano*, 2011, **5**, 2134–2134.
25 S. Pei, J. Zhao, J. Du, W. Ren and H.-M. Cheng, *Carbon*, 2010, **48**, 4466.
26 O. C. Compton, S. Kim, C. Pierre, J. M. Torkelson and S. T. Nguyen, *Adv. Mater.*, 2010, **22**, 4759.
27 R. H. Baughman, C. Cui, A. A. Zakhidov, Z. Iqbal, J. N. Barisci, G. M. Spinks, G. G. W. A. Mazzoldi, D. D. Rossi, A. G. Rinzler, O. J. S. Roth and M. Kertesz, *Science*, 1999, **284**, 1340.
28 L. Qiu, X. Yang, X. Gou, W. Yang, Z. F. Ma, G. G. Wallace and D. Li, *Chem.–Eur. J.*, 2010, **16**, 10653.
29 A. Mazzoldi, C. Degl'Innocenti, M. Michelucci and D. De Rossi, *Mater. Sci. Eng., C*, 1998, **6**, 65.
30 A. S. Hutchison, T. W. Lewis, S. E. Moulton, G. M. Spinks and G. G. Wallace, *Synth. Met.*, 2000, **113**, 121.
31 Y. Liu, B. Xie and Z. Xu, *J. Mater. Chem.*, 2011, **21**, 6707.
32 A. E. Aliev, J. Oh, M. E. Kozlov, A. A. Kuznetsov, S. Fang, A. F. Fonseca, R. Ovalle, M. D. Lima, M. H. Haque, Y. N. Gartstein, M. Zhang, A. A. Zakhidov and R. H. Baughman, *Science*, 2009, **323**, 1575.